

Shock ion acceleration by an ultrashort circularly polarized laser pulse via relativistic transparency in an exploded target

Young-Kuk Kim,¹ Myung-Hoon Cho,² Hyung Seon Song,³ Teyoun Kang,³ Hyung Ju Park,⁴ Moon Youn Jung,⁴ and Min Sup Hur^{3,*}

¹*School of Electrical and Computer Engineering, UNIST, 50 UNIST-gil, Ulsan-gun, Ulsan, 689-798, Korea*

²*Center for Relativistic Laser Science, Institute for Basic Science (IBS), Gwangju 500-712, Korea*

³*School of Natural Science, UNIST, 50 UNIST-gil, Ulsan-gun, Ulsan, 689-798, Korea*

⁴*Biomed Team, Electronics and Telecommunications Research Institute, 218 Gajeongno, Yuseong-gu, Daejeon 305-700, Korea*

(Received 27 March 2015; revised manuscript received 21 August 2015; published 6 October 2015)

We investigated ion acceleration by an electrostatic shock in an exploded target irradiated by an ultrashort, circularly polarized laser pulse by means of one- and three-dimensional particle-in-cell simulations. We discovered that the laser field penetrating via relativistic transparency (RT) rapidly heated the upstream electron plasma to enable the formation of a high-speed electrostatic shock. Owing to the RT-based rapid heating and the fast compression of the initial density spike by a circularly polarized pulse, a new regime of the shock ion acceleration driven by an ultrashort (20–40 fs), moderately intense (1–1.4 PW) laser pulse is envisaged. This regime enables more efficient shock ion acceleration under a limited total pulse energy than a linearly polarized pulse with crystal laser systems of $\lambda \sim 1 \mu\text{m}$.

DOI: [10.1103/PhysRevE.92.043102](https://doi.org/10.1103/PhysRevE.92.043102)

PACS number(s): 52.38.Kd, 52.35.Tc, 52.65.Rr

I. INTRODUCTION

The methods to generate MeV-class ion beams from interaction of intense laser and thin targets are attracting widespread interest from cancer therapy [1–4], material engineering [5,6], and proton imaging [7]. Those applications usually require the ion beams to be as monoenergetic as possible, in order to get a concentrated dose on the cancer cells or high-contrast imaging. For quasimonoenergetic ion beams from laser-target interaction, the technique of target-normal-sheath-acceleration (TNSA) combined with the second layer of light species [8–17] is available with a practical laser intensity such as $I \leq 10^{21} \text{ W/cm}^2$ [18]. Another scheme is radiation pressure acceleration (RPA), where the light pressure pushes an ultrathin ion layer continuously as a single quasimonoenergetic bunch in the light-sail regime [19–22]. However, the energy conversion efficiency is usually very low in TNSA. On the other hand, an ultrahigh contrast ratio more than 10^{-11} of the driving pulse is required in RPA. Furthermore RPA very often demands a pulse intensity beyond the feasible range of small-room-scale laser systems.

Recently it was suggested to use an electrostatic shock [23–30] for ion acceleration, where a laser pulse with moderate power and a near-critical target are used. In this system, a stable electrostatic shock with a high Mach number (> 1.5) is formed in a similar way as in Ref. [31]. As the shock is a highly positive, propagating ion density spike, a quasimonoenergetic ion beam can be generated through the reflection of incoming ions on the shock front. One essential condition for the shock formation is warm electrons [31], which is achieved via the recirculation [23] of hot electrons generated by the ponderomotive force of the driving pulse. Simultaneously the driving pulse makes an initial density spike of plasma moving with a piston velocity [25]. Another condition for the shock formation is that the piston velocity of the spike be large

enough to match the shock velocity. To meet this condition, the target density should be suitably low ($< 100n_c$) [23], which can be achieved by using a long wavelength (10 μm) CO₂ laser, along with a high-density gas instead of a solid target [29,32].

In this paper, we discovered another route to shock formation and related ion acceleration by a laser pulse with short wavelength ($\sim 1 \mu\text{m}$), moderate peak power (1.1–1.4 PW) and energy (28–42 J), ultrashort duration (20–40 fs), and circular polarization. To meet the low-density condition of the plasma, we employed an exploded target [33–35], where the plasma ionized primarily by the ASE or prepulse expands and its density decreases until the main pulse arrives. What we discovered is that the electron heating by relativistic transparency (RT) [36] can be an essential step for shock formation. This is contrasted to the conventional way of heating via an oscillating ponderomotive force of a linearly polarized wave and subsequent recirculation of the energetic electrons [23–29]. In the meantime, the reflected portion of the pulse energy contributes to the initial pistoning of an ion density spike. The penetrating electromagnetic field heats the electrons rapidly compared to the electron recirculation process, allowing the use of an ultrashort pulse of several tens of femtoseconds. On the other hand the circular polarized pulse can piston the initial density spike to the required Mach number faster than the linear one with the same energy. Consequently the circularly polarized pulse can be more efficient than the linear one in shock ion acceleration under the limited pulse energy. In our scheme, controlled prepulse energy and duration are utilized for target explosion [30].

This paper is organized as follows. An RT-based shock acceleration is shown through one-dimensional simulations in Sec. II. A three-dimensional simulation is presented in Sec. III. The conclusion is given in Sec. IV.

II. ONE-DIMENSIONAL SIMULATIONS

From one-dimensional particle-in-cell (PIC) simulations, we observed that direct electron heating by the laser penetration developed a Mach number larger than 1.5, resulting

*mshur@unist.ac.kr

in high shock velocity ($\sim 0.2c$), using a 1.4 PW, 20 fs laser pulse. The shock formation and ion acceleration could also be observed in full three-dimensional PIC simulations with slightly different laser and plasma parameters.

For the one-dimensional PIC simulations using a verified code [37–39], a circularly polarized Gaussian laser pulse with $\lambda = 1 \mu\text{m}$, τ (pulse duration) = 20 fs, and a_0 (normalized vector potential) = 18 was launched from the left side of the simulation box, which was $40 \mu\text{m}$ long, divided by 1 nm meshes. To model the density profile of the initially rectangular, vacuum-expanding plasma, we adopted a formula obtained from the hydrocalculation in Ref. [33]:

$$n_i(x) = \frac{2n_{i,\text{max}}}{1 + \exp\left[\frac{2v\theta(v)}{l_f} - \frac{2v\theta(-v)}{l_f}\right]}, \quad (1)$$

where $v = x - 0.5l_0$ and $\theta(x)$ is the step function. The parameters n_i , $n_{i,\text{max}}$, l_f , l_r , and l_0 are the plasma density, the maximum plasma density, the front and backside scale lengths of the density, and the initial target thickness, respectively. For a target with $l_0 = 30 \text{ nm}$ and $n_0 = 600n_c$ located at $X = 20 \mu\text{m}$, we conducted the simulations with three different levels of expansion with $l_f = l_r = 1, 2$, and $3 \mu\text{m}$. Corresponding peak densities were $n_{e,\text{max}} = 13, 6.5$, and $4.3n_c$, respectively, from integration of Eq. (1) [$\int n_i dx = n_0 l_0 / (l_{fr} + l_r) / \ln 2$]. We assumed a fully ionized carbon plasma (C^{6+}). The number of particles per cell per species was 200 at the maximum density, which was sufficiently large to suppress numerical heating and to represent the tail part of the plasma density with a large enough number of macro particles.

Figure 1 is the representative one-dimensional result, illustrating the new procedure of shock formation well. The left column exhibits three steps of shock formation: (a) density spike formed by the ponderomotive force of the circularly polarized pulse, (b) partial transparency of the pulse energy by the relativistic effect and related electron heating, and (c) shock formation after leaving of the transparent pulse and ion acceleration. In step (a), the velocity of the density spike moves with a piston velocity, which is comparable to the shock velocity, which appears later, but it is not a shock yet: the charge is almost neutral, which indicates that it is just a compressed bunch of ions and electrons. The evidences for the RT-induced electron heating in step (b) can be found from Fig. 1(d). For $l_f = 2$ and $3 \mu\text{m}$, where the target densities are low enough to induce RT, the electron temperature in the upstream increases significantly up to several MeV. The temperature increment begins from $t = 120$ fs, which is coincident with the start of RT [Fig. 1(a)]. Meanwhile the electron temperature remains noticeably cold at around 400 keV for $l_f = 1 \mu\text{m}$, where the target density is too high to induce RT. In our simulations, the electron density in the density spike for $l_f = 2$ and $3 \mu\text{m}$ was lower than the RT threshold approximately given by $\sqrt{1 + a_0^2} n_c \simeq 18n_c$, while it was not for $l_f = 1 \mu\text{m}$. Such a heating mechanism by the relativistic transparency is different from that of previous works in Refs. [23–29], where the electron recirculation by the reflection from the sheath field dominates. Note that step (c) occurs only after complete leaving of the pulse, indicating the shock is electrostatic. This is a different feature from that of Yin *et al.* [36], where

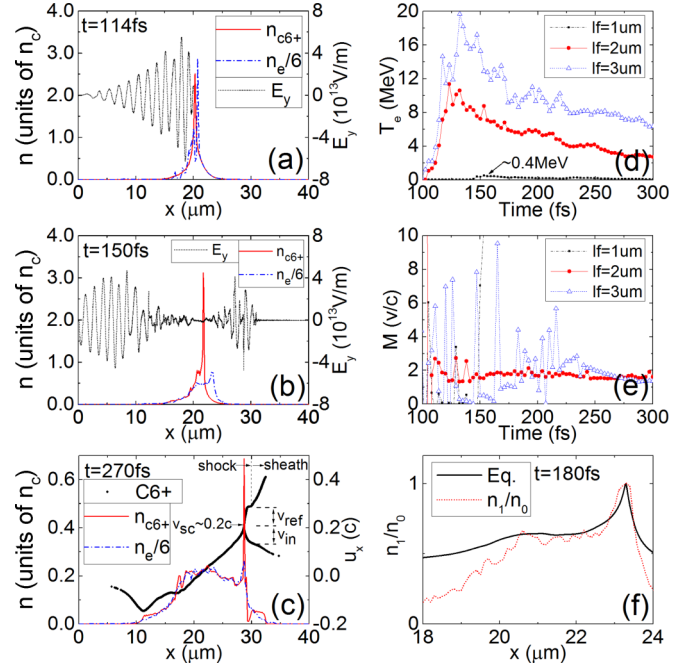


FIG. 1. (Color online) One dimensional simulations with $a_0 = 18$, circular polarization, and pulse duration 20 fs. $l_f = 2 \mu\text{m}$ for (a)–(c) and (f). (a) Compression of initial density spike, (b) during RT, and (c) after RT along with the ion phase space. (d) Average electron temperature in the upstream for different l_f and (e) Mach numbers. (f) Comparison of Eq. (2) and simulation data for $l_f = 2 \mu\text{m}$.

an electromagnetic solitary wave is generated during the interaction between the laser field and plasma.

The existence of the shock could also be qualitatively verified from the measurement of Mach number of the density spike and velocity doubling of incident ions in the phase space. Figure 1(e) represents the Mach numbers of the density spikes for three different cases ($l_f = 1, 2, 3 \mu\text{m}$). From Ref. [31], the Mach number of the laminar electrostatic shock should be $1.5 < M < 3.5$, which is satisfied by the $l_f = 2 \mu\text{m}$ case ($M \sim 1.6$). The velocity doubling by the reflection of incident ions can also be found in Fig. 1(c). As the shock collects ions in front of it via reflection, a distinct density bump is formed beyond $X = 30 \mu\text{m}$. Those typical characteristics of shock acceleration could not be observed in the cases with $l_f = 1$ or $3 \mu\text{m}$.

In order to demonstrate more rigorously that the density spike in Fig. 1 is actually a laminar electrostatic shock, we compared the density profile from the simulation with the following equation suggested by Forslund *et al.* [31], which relates the electron density, and potential difference in the downstream:

$$\frac{n_1}{n_0} = 2\psi/\sqrt{\pi} + e^\psi \text{erfc}(\sqrt{\psi}), \quad (2)$$

where $\psi = e\varphi/kT_e$, φ is the potential, T_e is the upstream electron temperature, n_1 is the downstream density, and $\text{erfc}(x)$ is the complement error function. As can be seen from Fig. 1(f), this equation coincides well with the density in the downstream from $X = 20.5$ to $23.5 \mu\text{m}$ measured from the simulation with $l_f = 2 \mu\text{m}$. We could not find any good match between Eq. (2)

and the simulation results for $l_f = 1$ and $3 \mu\text{m}$, implying they are not actually shocks.

One interesting aspect of the exploded target is that the created shock can be sustained for a long time in the decreasing plasma density even in the absence of the laser pressure. For the exploded target, which has an exponentially decreasing density profile in the backside, the number of incident ions on the shock front is considerably reduced compared to the uniform case. Hence, the shock structure can propagate in the plasma without significant momentum loss, which enables it to sustain the shock even without the driving laser pulse. For $l_f = 2 \mu\text{m}$, it is found that the shock velocity is reduced just slightly even after complete leaving of the laser field at $t = 200$ fs. The final shock velocity is about $0.2c$, which does not deviate significantly from the initial piston velocity. On the other hand, in the $l_f = 1 \mu\text{m}$ case, the velocity of the ion density spike is constant at $0.17c$ throughout the simulation, which indicates that there is no momentum transfer at all from the spike to the background ions. In this case, abundant cold electrons quickly shield the reflecting field from the ion density spike, which is generated in the early hole-boring stage, and they just ballistically propagate without the driving laser pressure.

Extremely high electron temperatures can prohibit the shock formation (the case of $l_f = 3 \mu\text{m}$). Highly energetic electrons easily escape the shock potential, showing an oscillating behavior [25]. Accordingly the electrostatic field also oscillates, which eventually smears out the density spike of the shock. Approximately $q\phi > 0.5\gamma m_e v_e^2$ is one of the necessary conditions for stable shock formation. To check this from our simulations, we measured the potential difference and the average kinetic energy of electrons over the position between the density peak and $1.5 \mu\text{m}$ away from that, which was sufficiently wide to cover the Debye length around the density spike. These measurement are summarized in Table I. For $l_f = 3 \mu\text{m}$, where the relativistic transparency is strongest and the temperature is two times higher than that for the $l_f = 2 \mu\text{m}$ case, the electron's kinetic energy is higher than the potential energy, ending up with smeared-out shock eventually.

From Fig. 2, it is clear that the $l_f = 2 \mu\text{m}$ case yielded the best ion beam acceleration among three exploded targets. An ion beam over 400 MeV, originating from the reflected ions on the shock front, is well separated from the thermal beam under 300 MeV. The latter is from the shock itself and the downstream ions. Due to the combination of the shock and sheath acceleration, $l_f = 2 \mu\text{m}$ plasma generated the highest maximum ion energy at 780 MeV. Another interesting feature is that the shock itself contains a quasimonoenergetic peak at 240 MeV, which is relatively high compared with 180 MeV

TABLE I. Average gamma factor of electrons, average electron kinetic energy E_k near the ion density peak, and potential difference from the ion density peak to $1.5 \mu\text{m}$ away from that, at $t = 180$ fs. In the case of $l_f = 3 \mu\text{m}$, $\Delta\phi - E_k < 0$.

l_f (μm)	γ	E_k (MeV)	$\Delta\phi$ (MeV)	$\Delta\phi - E_k$
1	1.1	0.05	2	+
2	20	10	20	+
3	60	30	15	-

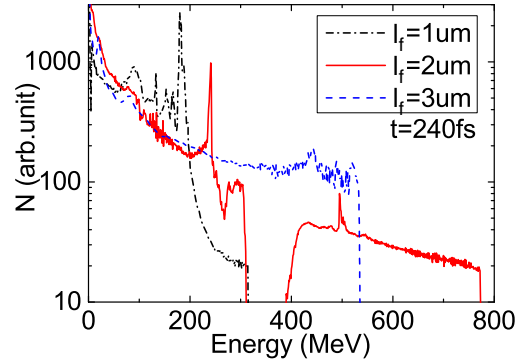


FIG. 2. (Color online) Energy spectra of the accelerated ion beams for three different cases: $l_f = 1, 2,$ and $3 \mu\text{m}$ at $t = 240$ fs.

from the RPA-dominant case with $l_f = 1 \mu\text{m}$. When the transparency of the laser pulse was too high ($l_f = 3 \mu\text{m}$), the high electron temperature led to a thermal energy spectrum of the ion beam.

When the laser pulse intensity increases from $a_0 = 18$ to $a_0 = 22$ keeping other parameters the same as in the $l_f = 2 \mu\text{m}$ case, the RT effect increases to yield a similar oscillating behavior of Mach number (see Fig. 3) as in the previous $l_f = 3 \mu\text{m}$ case with $a_0 = 18$. In this case, the shock diminishes quickly even for a higher driving power (see the inset). On the other hand, when the laser pulse intensity decreases from $a_0 = 18$ to $a_0 = 10$ the shock acceleration turns into RPA dominant process (not shown here).

When the same ultrashort laser pulse is linearly polarized, no meaningful density spike could be observed in our supplemental simulations for $a_0 = 10$ – 25.5 . Usually such a longer pulse is required in the linearly polarized case so as to push the density spike deep into the higher-density target. However, under the same total pulse energy, the peak intensity of the pulse should be decreased as the pulse duration is prolonged, which may yield much decreased ion energy. When the pulse duration is prolonged to 1 ps under our simulation conditions, a_0 becomes 2.5 . From the scaling law of the ion energy presented in Ref. [28], the optimized carbon ion energy driven by a linearly polarized pulse is less than 100 MeV,

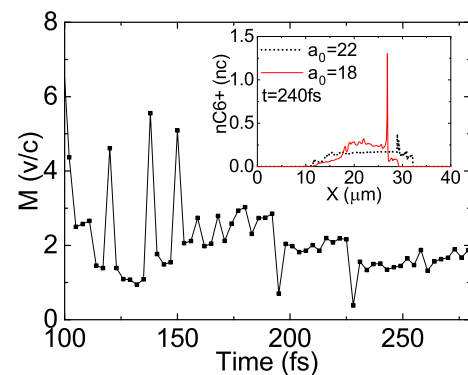


FIG. 3. (Color online) Mach number oscillation for increased laser intensity from $a_0 = 18$ to 22 for $l_f = 2 \mu\text{m}$. Inset represents the density spikes for $a_0 = 22$ (dotted black line) and 18 (solid red line).

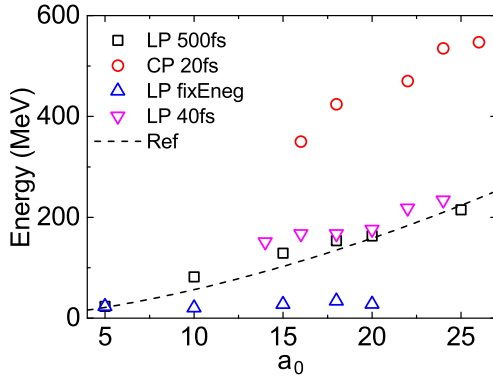


FIG. 4. (Color online) Scaling of ion (C^{6+}) energy as a function of laser amplitude, obtained from one-dimensional PIC simulations. Four different cases are presented; circularly polarized (CP) pulses with $\tau = 20$ fs and $l_f = 2$ μm (circles), where τ is the pulse duration. They can be directly compared with the linearly polarized (LP) pulses with $\tau = 40$ fs and $l_r = 2$ μm (inverted triangles). LP pulses with $\tau = 500$ fs and exponential plasma tail in the rear side with $l_r = 20$ μm (squares). LP pulses with varying a_0 and τ , keeping the pulse energy ($\sim a_0^2 \tau$) constant by that of $a_0 = 18$ and $\tau = 20$ fs case of CP, and with $l_r = 20$ μm (triangles). Dashed line represents the ion energy scaling law from Ref. [28] for $\tau = 500$ fs, C^{6+} ion, and $l_r = 20$ μm .

which is significantly smaller than that in Fig. 2. Furthermore, the reduction of the target density should be accompanied to the lowered a_0 , which will inevitably decrease the accelerated beam charge.

It is found from Fig. 4 that the RT-based shock is quite robust for a broad range of laser and target parameters. In this figure, one-dimensional PIC simulations for the ion energy versus the amplitude a_0 of the driver pulse is presented. In each case the target parameters are arranged so that the shock is formed properly. The higher the ion energy is for the stronger laser intensity, as the hole-boring speed and accordingly the shock velocity increases. In addition, a comparison with the cases from linearly polarized (LP) pulses with the same pulse energy is presented. In LP cases, usually a higher plasma density is required to compress the density spike by preventing the transparency. Thus the HB velocity is slower in LP cases, leading to lower ion energies (but obviously a higher beam charge from the high-density plasma). Note that the LP cases follow well the scaling law from Ref. [28], denoted by a dashed line in the figure.

Throughout our simulations, we used 1 μm for the wavelength of the driver laser pulse. A more practical wavelength of the short laser pulse may be at around 800 nm from a Ti:sapphire laser system. The relativistic transparency, which is suggested as one of the major steps for the shock formation, is determined dominantly by the electron density. Hence we expect a slight scaling up of the target density and pulse intensity for a reduced wavelength to 800 nm would yield almost the identical results.

III. THREE-DIMENSIONAL SIMULATIONS

The RT-based shock formation and ion acceleration could also be observed in three-dimensional, full PIC simulations. In

multidimensional systems, the parameters for the stable shock formation should be different from those in one-dimensional systems, as additional instabilities interrupt the piling up of the density spike in the early stage. For instance, we observed that the Weibel-like instability [40] grew rapidly for $l_f = 2$ μm , resulting in early destruction of the density spike by severe filamentation. Reducing the interaction time by shortening the front scale length l_f helps to mitigate the filamentation. Also, a gently rising pulse front is known to be effective in keeping the density spike stable for a long time [41]. As another adjustment for robust shock formation, the pulse tail was shortened so that the density spike was less perturbed by the penetrating laser field by RT.

Simulation parameters considering all those factors are $l_f = 0.33$ μm , $l_r = 0.45$ μm , and $n_{\text{max}} = 15.6n_c$ (corresponding to $l_0 = 13.7$ nm and $n_0 = 600n_c$ before the explosion), and an asymmetric laser pulse with $a_0 = 16$, pulse rising for 27 fs, falling for 11 fs, and the spot radius 10 μm , respectively. The dimensions of the simulation box were $10 \times 50 \times 50$ [μm] in the X , Y , and Z directions, divided by meshes of 10, 100, and 100 nm in each direction. The simulation results using those parameters are presented in Fig. 5. Figure 5(a) is the snapshot of the ion density captured at $t = 120$ fs at which the laser pulse has completely left the plasma. The concentrated region (dark red) of the density represents the shock. From the electric field drawn on the upper plane, it is found that there are two accelerating fields: one is the shock itself, and the other is the sheath. The branch in the ion phase space [Fig. 5(b)] in front of the density spike near the laser axis is a result of velocity doubling by the reflection of incoming ions from the shock front. The number of reflected ions within the laser spot radius 10 μm is $N_{\text{ions}} \sim 7 \times 10^{10}$. This value is comparable to the formula $N_{\text{ions}} \sim 10^{10}(W_0 [\mu\text{m}]/\lambda_0 [\mu\text{m}])$ in Ref. [28], where W_0 is the laser spot radius. The measured efficiency of energy conversion from the laser pulse to the accelerated ions is 4.3%. The Mach number becomes $M < 4$ at $t = 70$ fs and is maintained at around $M \simeq 2$ until $t = 150$ fs [Fig. 5(c)], during which time the ion acceleration continuously takes place. The laser penetration starts at $t = 70$ fs and completes the laser-plasma interaction at $t = 113$ fs. The slightly distinct second bump above 60 MeV in the ion energy spectrum in Fig. 5(d) takes a similar feature as the one-dimensional result in Fig. 2.

Note that the asymmetric target profile with slightly longer rear side used in the three-dimensional simulation may not be easy to realize in the laboratory. However, the shock is formed dominantly in the front side, so the rear side dimension is not so influential. The rear side tail, as described in Ref. [28], is used usually for the sheath control. As the sheath effect can be suppressed by a longer tail in the rear, the symmetric target with a shorter l_r in our three-dimensional simulation should have resulted in slightly increased maximum energy of ions and more energy spread by the increased sheath effect.

IV. CONCLUSION

In summary, by one- and three-dimensional PIC simulations, we revealed a new procedure of electrostatic shock formation by relativistic transparency (RT) in exploded targets

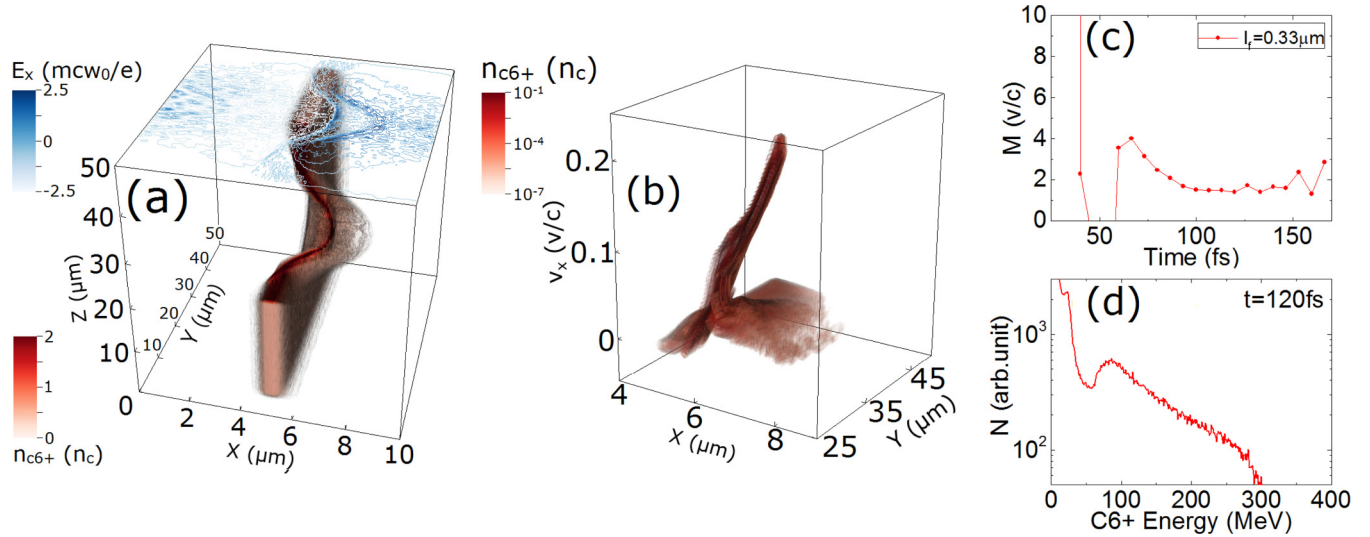


FIG. 5. (Color online) Three dimensional PIC simulation with $a_0 = 16$, circular polarization, $\tau_f = 33$ fs and $\tau_r = 13$ fs, and $l_f = 0.33 \mu\text{m}$. (a) Ion density and longitudinal field E_x on $Z = 25 \mu\text{m}$ plane (which is drawn on the upper side of the box) after leaving the laser field at $t = 120$ fs. (b) The half cut of a $V_x XY$ -phase space of ions. (c) Temporal evolution of the Mach number. (d) Ion energy spectrum at $t = 120$ fs.

and related ion acceleration. In this procedure, the penetrating laser field by RT rapidly heats up the electron plasma, providing the upstream with the condition of high sound speed. Reduction of the target plasma density to induce RT of a circularly polarized pulse could be achieved by expansion of the exploded targets. The partially reflecting portion of the pulse drives an initial density spike to piston velocity via the hole-boring mechanism. When the reflected and transparent portions of the driving pulse are properly chosen, the Mach number of the initial density spike satisfies the shock criterion, i.e., $M > 1.5$, turning it into an electrostatic shock. The shock could be sustained for a long time even in the absence of the driving pulse, owing to the tapered density of the expanded target. The ions in the upstream are reflected from the shock front to constitute a localized energetic ion bunch. In a certain case the shock front itself contained a monoenergetic portion of the ions.

The rapid electron heating by the transparent field allows the use of a short driving pulse of a few tens of femtoseconds. Using a circularly polarized pulse significantly relaxes the demands for high pulse power required for compression of the

initial density spike, i.e., down to 1 PW (or slightly larger). Ti:sapphire laser systems with those parameters are readily available with contemporary technology. Furthermore the controlled ASE or prepulse is utilized for target explosion to induce a suitable RT. The relativistic transparency can be controlled by using the target expansion level, which is possible in the experiment using ASE or a prepulse, or by changing the initial target thickness for a given ASE. Those specifications envisages a new parameter regime of shock ion acceleration.

ACKNOWLEDGMENTS

This work was supported by the ICT R&D program of MSIP/IITP (10035602, Core Technology Development of Laser Accelerated Ion-Beam Generation System for Cancer Therapy) and partially by the Basic Science Research Program through the National Research Foundation (NRF) of Korea funded by the Ministry of Science, ICT and Future Planning (Grant No. NRF-2013R1A1A2006353). For the simulations, we were supported by the PLSI supercomputing resources of the Korea Institute of Science and Technology Information.

- [1] S. V. Bulanov, T. Zh. Esirkepov, V. S. Khoroshkov, A. V. Kuznetsov, and F. Pegoraro, *Phys. Lett. A* **299**, 240 (2002).
- [2] E. Fourkal, I. Velchev, J. Fan, W. Luo, and C.-M. Ma, *Med. Phys.* **34**, 577 (2007).
- [3] V. Malka, S. Fritzler, E. Lefebvre, E. d'Humières, R. Ferrand, G. Grillon, C. Albaret, S. Meyroneinc, J.-P. Chambaret, A. Antonetti, and D. Hulin, *Med. Phys.* **31**, 1587 (2004).
- [4] T. Tajima and G. Mourou, *Phys. Rev. Spec. Top.-Accel.* **5**, 031301 (2002).
- [5] L. Torrisi, S. Gammino, A. M. Mezzaslima, J. Badziak, P. Parys, J. Wolowski, E. Woryna, J. Krása, L. Láska, M. Pfeifer, K. Rohlena, and F. P. Boody, *Appl. Surf. Sci.* **217**, 319 (2003).
- [6] F. P. Boody, R. Höpfl, H. Hora, and J. C. Kelly, *Laser Part. Beams* **14**, 443 (1996).
- [7] M. Borghesi, A. Schiavi, D. H. Campbell, M. G. Haines, O. Willi, A. J. MacKinnon, L. A. Gizzi, M. Galimberti, R. J. Clarke, and H. Ruhl, *Plasma Phys. Control. Fusion* **43**, A267 (2001).
- [8] J. Fuchs, P. Antici, E. d'Humières, E. Lefebvre, M. Borghesi, E. Brambrink, C. A. Cecchetti, M. Kaluza, V. Malka, M. Manclossi, S. Meyroneinc, P. Mora, J. Schreiber, T. Toncian, H. Pépin, and P. Audebert, *Nat. Phys.* **2**, 48 (2006).
- [9] M. Passoni, L. Bertagna, and A. Zani, *New J. Phys.* **12**, 045012 (2010).
- [10] L. Robson, P. T. Simpson, R. J. Clarke, K. W. D. Ledingham, F. Lindau, O. Lundh, T. McCanny, P. Mora, D. Neely,

- C.-G. Wahlström, M. Zepf, and P. McKenna, *Nat. Phys.* **3**, 58 (2007).
- [11] S. C. Wilks, A. B. Langdon, T. E. Cowan, M. Roth, M. Singh, S. Hatchett, M. H. Key, D. Pennington, A. MacKinnon, and R. A. Snavely, *Phys. Plasmas* **8**, 542 (2001).
- [12] J. Badziak, E. Woryna, P. Parys, K. Yu. Platonov, S. Jabłoński, L. Ryć, A. B. Vankov, and J. Wołowski, *Phys. Rev. Lett.* **87**, 215001 (2001).
- [13] T. Zh. Esirkepov, S. V. Bulanov, K. Nishihara, T. Tajima, F. Pegoraro, V. S. Khoroshkov, K. Mima, H. Daido, Y. Kato, Y. Kitagawa, K. Nagai, and S. Sakabe, *Phys. Rev. Lett.* **89**, 175003 (2002).
- [14] B. M. Hegelich, B. J. Albright, J. Cobble, K. Flippo, S. Letzring, M. Paffett, H. Ruhl, J. Schreiber, R. K. Schulze, and J. C. Fernández, *Nature (London)* **439**, 441 (2006).
- [15] E. Fourkal, I. Velchev, and C.-M. Ma, *Phys. Rev. E* **71**, 036412 (2005).
- [16] H. Schwoerer, S. Pfoth, O. Jäckel, K.-U. Amthor, B. Liesfeld, W. Ziegler, R. Sauerbrey, K. W. D. Ledingham, and T. Esirkepov, *Nature (London)* **439**, 445 (2006).
- [17] J. Q. Yu, X. L. Jin, W. M. Zhou, B. Zhang, Z. Q. Zhao, L. F. Cao, B. Lin, Y. Q. Gu, R. X. Zhan, and Z. Najmudin, *Laser Part. Beams* **31**, 597 (2013).
- [18] I. J. Kim, K. H. Pae, C. M. Kim, H. T. Kim, J. H. Sung, S. K. Lee, T. H. Yu, I. W. Choi, C.-L. Lee, K. H. Nam, P. V. Nickles, T. M. Jeong, and J. M. Lee, *Phys. Rev. Lett.* **111**, 165003 (2013).
- [19] T. Esirkepov, M. Borghesi, S. V. Bulanov, G. Mourou, and T. Tajima, *Phys. Rev. Lett.* **92**, 175003 (2004).
- [20] N. P. Dover and Z. Najmudin, *High Energy Density Phys.* **8**, 170 (2012).
- [21] A. Henig, S. Steinke, M. Schnürer, T. Sokollik, R. Hörlein, D. Kiefer, D. Jung, J. Schreiber, B. M. Hegelich, X. Q. Yan, J. Meyer-ter-Vehn, T. Tajima, P. V. Nickles, W. Sandner, and D. Habs, *Phys. Rev. Lett.* **103**, 245003 (2009).
- [22] B. Qiao, M. Zepf, M. Borghesi, and M. Geissler, *Phys. Rev. Lett.* **102**, 145002 (2009).
- [23] L. O. Silva, M. Marti, J. R. Davies, R. A. Fonseca, C. Ren, F. S. Tsung, and W. B. Mori, *Phys. Rev. Lett.* **92**, 015002 (2004).
- [24] M. Chen, Z.-M. Sheng, Q.-L. Dong, M.-Q. He, S.-M. Weng, Y.-T. Li, and J. Zhang, *Phys. Plasmas* **14**, 113106 (2007).
- [25] A. Macchi, A. S. Nindrayog, and F. Pegoraro, *Phys. Rev. E* **85**, 046402 (2012).
- [26] H. Y. Wang, C. Lin, B. Liu, Z. M. Sheng, H. Y. Lu, W. J. Ma, J. H. Bin, J. Schreiber, X. T. He, J. E. Chen, M. Zepf, and X. Q. Yan, *Phys. Rev. E* **89**, 013107 (2014).
- [27] A. Zhidkov, M. Uesaka, A. Sasaki, and H. Daido, *Phys. Rev. Lett.* **89**, 215002 (2002).
- [28] F. Fiuza, A. Stockem, E. Boella, R. A. Fonseca, L. O. Silva, D. Haberberger, S. Tochitsky, C. Gong, W. B. Mori, and C. Joshi, *Phys. Rev. Lett.* **109**, 215001 (2012).
- [29] D. Haberberger, S. Tochitsky, F. Fiuza, C. Gong, R. A. Fonseca, L. O. Silva, W. B. Mori, and C. Joshi, *Nat. Phys.* **8**, 95 (2012).
- [30] H. Zhang, B. F. Shen, W. P. Wang, Y. Xu, Y. Q. Liu, X. Y. Liang, Y. X. Leng, R. X. Li, X. Q. Yan, J. E. Chen, and Z. Z. Xu, *Phys. Plasmas* **22**, 013113 (2015).
- [31] D. W. Forslund and C. R. Shonk, *Phys. Rev. Lett.* **25**, 1699 (1970).
- [32] C. A. J. Palmer, N. P. Dover, I. Pogorelsky, M. Babzien, G. I. Dudnikova, M. Ispiryan, M. N. Polyanskiy, J. Schreiber, P. Shkolnikov, V. Yakimenko, and Z. Najmudin, *Phys. Rev. Lett.* **106**, 014801 (2011).
- [33] A. A. Andreev, S. Steinke, T. Sokollik, M. Schnürer, and S. T. Avetsiyan, *Phys. Plasmas* **16**, 013103 (2009).
- [34] A. Yogo, H. Daido, S. V. Bulanov, K. Nemoto, Y. Oishi, T. Nayuki, T. Fujii, K. Ogura, S. Orimo, A. Sagisaka, J.-L. Ma, T. Zh. Esirkepov, M. Mori, M. Nishiuchi, A. S. Pirozhkov, S. Nakamura, A. Noda, H. Nagatomo, T. Kimura, and T. Tajima, *Phys. Rev. E* **77**, 016401 (2008).
- [35] E. d'Humières, P. Antici, M. Glesser, J. Boeker, F. Cardelli, S. Chen, J. L. Feugeas, F. Filippi, M. Gauthier, A. Levy, P. Nicolai, H. Pépin, L. Romagnani, M. Scisciò, V. T. Tikhonchuk, O. Willi, J. C. Kieffer, and J. Fuchs, *Plasma Phys. Control. Fusion* **55**, 124025 (2013).
- [36] L. Yin, B. J. Albright, D. Jung, K. J. Bowers, R. C. Shah, S. Palaniyappan, J. C. Fernández, and B. M. Hegelich, *Phys. Plasmas* **18**, 053103 (2011).
- [37] I. H. Nam, M. S. Hur, H. S. Uhm, N. A. M. Hafz, and H. Y. Suk, *Phys. Plasmas* **18**, 043107 (2011).
- [38] M. S. Hur, Y.-K. Kim, V. V. Kulagin, I. H. Nam, and H. Y. Suk, *Phys. Plasmas* **19**, 073114 (2012).
- [39] M.-H. Cho, Y.-K. Kim, and M. S. Hur, *Phys. Plasmas* **20**, 093112 (2013).
- [40] X. M. Zhang, B. F. Shen, L. L. Ji, W. P. Wang, J. C. Xu, Y. H. Yu, and X. F. Wang, *Phys. Plasmas* **18**, 073101 (2011).
- [41] L. L. Ji, B. F. Shen, X. M. Zhang, F. C. Wang, Z. Y. Jin, X. M. Li, M. Wen, and J. R. Cary, *Phys. Rev. Lett.* **101**, 164802 (2008).